SUPPLEMENTARY FIGURES

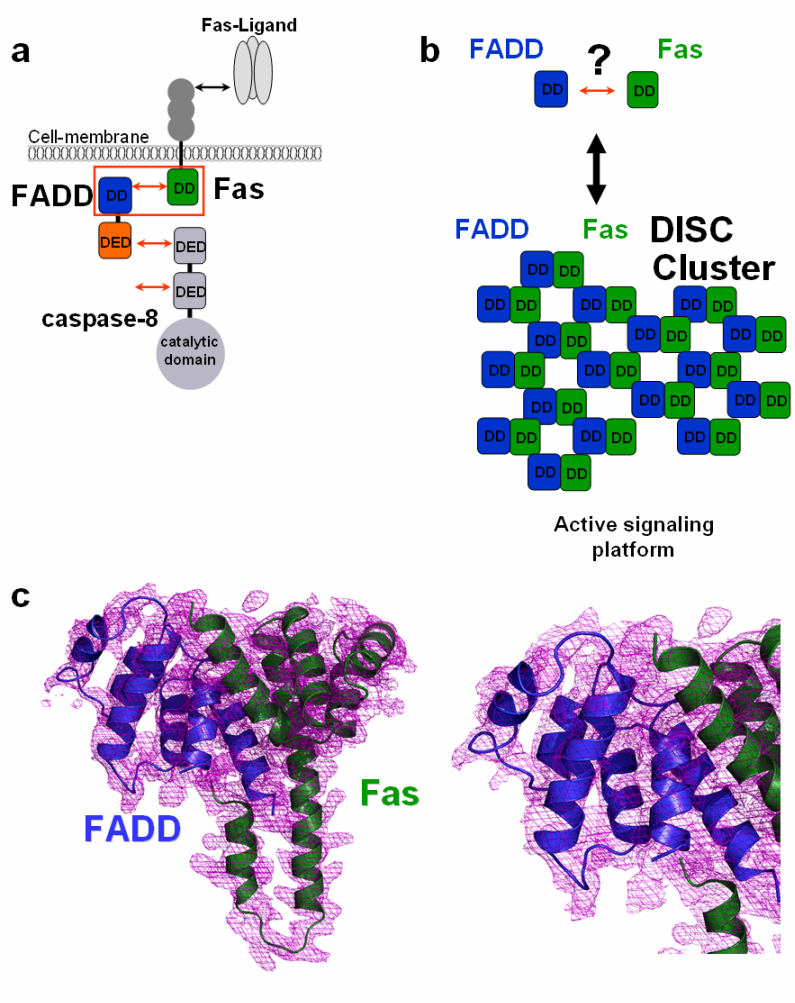

Supplementary Figure 1 | The Fas/FADD complex – core of the DISC. a, Simplified schematic of DISC interactions. DISC signaling is mediated by death domain interactions. In a simplified view the binding of Fas ligand to Fas receptor leads to the recruitment of FADD via DD interactions. FADD in turn recruits caspase-8 via interactions utilizing the DEDs of both proteins, leading to activation of the caspase. **b,** The Fas/FADD DD interaction is at the center of DISC clusters, which represent the actual active signaling platform. Although known to form an essential complex, single death domains of Fas and FADD do not and should not readily interact, which is reflected in the elusiveness of the complex. However, stable complex formation does occur within the DISC and at the same time acts as the central building block of DISC clusters. **c.** Electron-density map of the primary Fas/FADD DD complex. 2Fo-Fc map of the primary complex with residues comprising helices 3,4 (left) and 4,5 (right; close up) of FADD omitted for the calculation of the map (contoured at 0.8 σ).

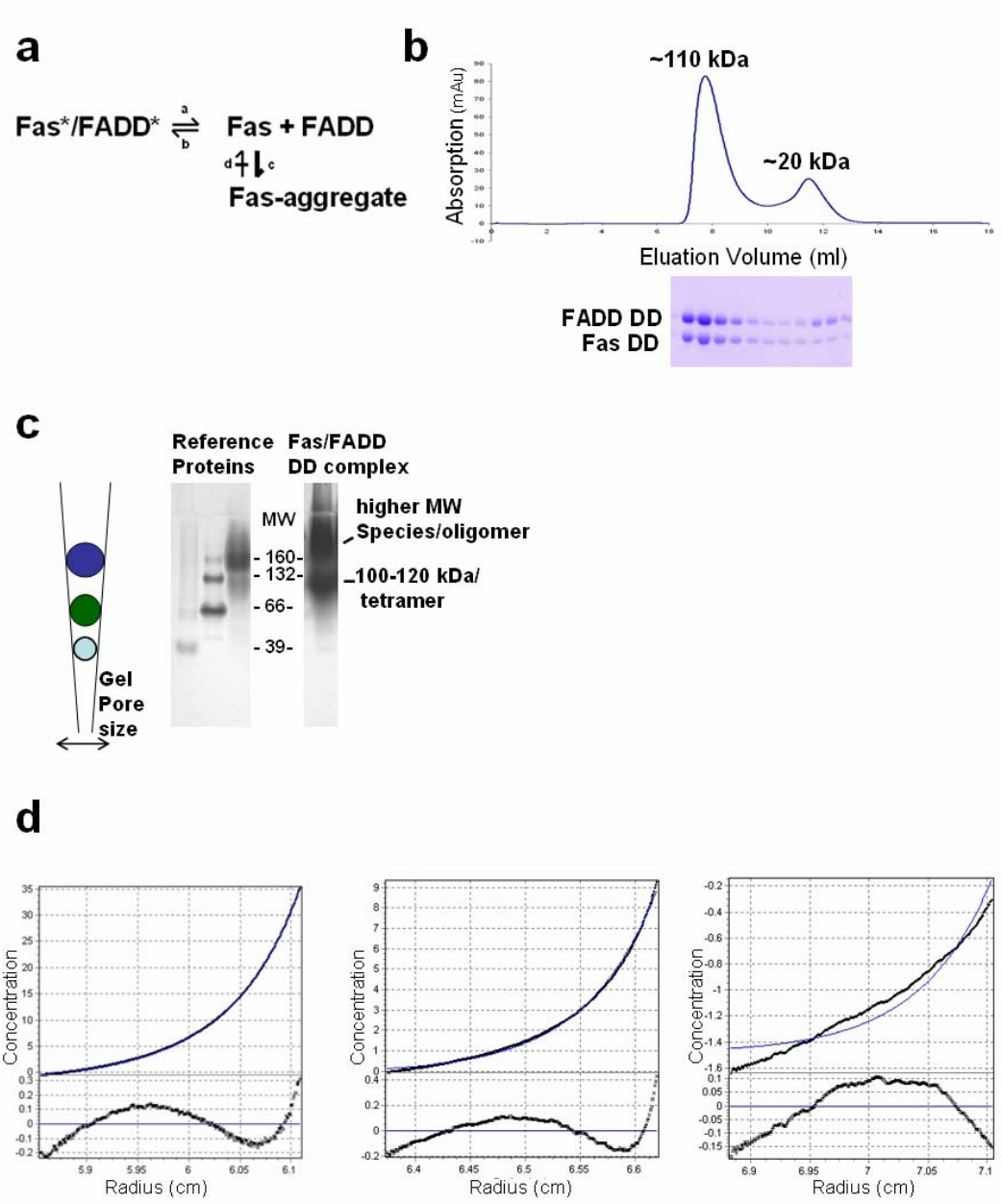

Supplementary Figure 2 | The Fas/FADD interaction is multifaceted and weak. a, Intricate interaction patterns and solubility problems limit biochemical analysis. Displayed is a simplified schematic illustrating kinetic constants in the Fas/FADD DD complex formation/dissociation. Unlike a simple one step formation, the Fas/FADD complex formation in solution is characterized by many multiple events (indicated by *), such as conformational changes in Fas, Fas/FADD encounter complexes, dimerization and tetramerization events. Additionally the notorious tendency of unbound Fas to self-aggregate at

concentrations needed to form the weak primary Fas/FADD complex severely limit biochemical analysis. Thus methods visualizing individual protein/complex species and simultaneously indicating their size, such as gel filtration and pore size limiting PAGE are necessary for characterization. **b,** Gel filtration analysis of the Fas/FADD DD complex after isolation by ion-exchange chromatography**.** The Fas/FADD complex shows an apparent molecular weight resembling a tetramer of four Fas/FADD DD complexes. The strong tendency of the complex to dissociate is evidenced by the presence of the individual components in fractions corresponding to smaller size. **c,** Analysis of the Fas/FADD DD complex by size-limiting PAGE. (left) Schematic illustrating the principle of size-limiting PAGE. A defined poly acrylamide pore size gradient allows proteins to migrate through the gel until arrested at a position dependent on the size of the protein. This method is independent of the overall charge of the protein, providing a feasible instrument to assess the size of a complex and at the same time observe the presence of multiple species, such as additional oligomers[31]. (center) Reference containing proteins of known size (lines 1 to 3: CrmA, BSA and Transferrin). (right) The Fas/FADD DD complex shows an apparent size of ~100-120 kDa, supporting a tetramer of Fas/FADD DD complexes. Additionally the tendency of the complex to form higher-oligomers is captured by the gel pores. **d,** Analysis of the Fas/FADD DD complex by analytical ultracentrifugation. Sedimentation equilibrium data (black line) were fitted to a single ideal species model (blue line). Several complex concentrations were analyzed, data is shown for three concentrations. Plots of the residuals for each data set are shown below. The best fit was achieved for the sample containing a protein concentration of 370 μM (left; concentration referring to one Fas and one FADD DD as unit), which yielded an overall MW of ~133 kDa for the sample. A similar result was obtained for a sample containing a protein concentration of 125 μM (middle), although the fit was less accurate. This AUC points to the presence of a tetrameric complex at high protein concentrations, given that the somewhat higher than predicted experimental MW (133 vs. 108 kDa) is likely a result of the presence of higher oligomers, since residuals for the 370 μM and 125 μM data sets show characteristic aggregation signs. The data for a protein concentration of 40 μM (right) could not be fit to the single ideal species model. The shape of this distribution indicates complex dissociation at this concentration which is even more evident at protein concentrations of 13 μM, 4.5 μM and 1.5 μM (data not shown) as expected for the weak Fas/FADD DD complex.

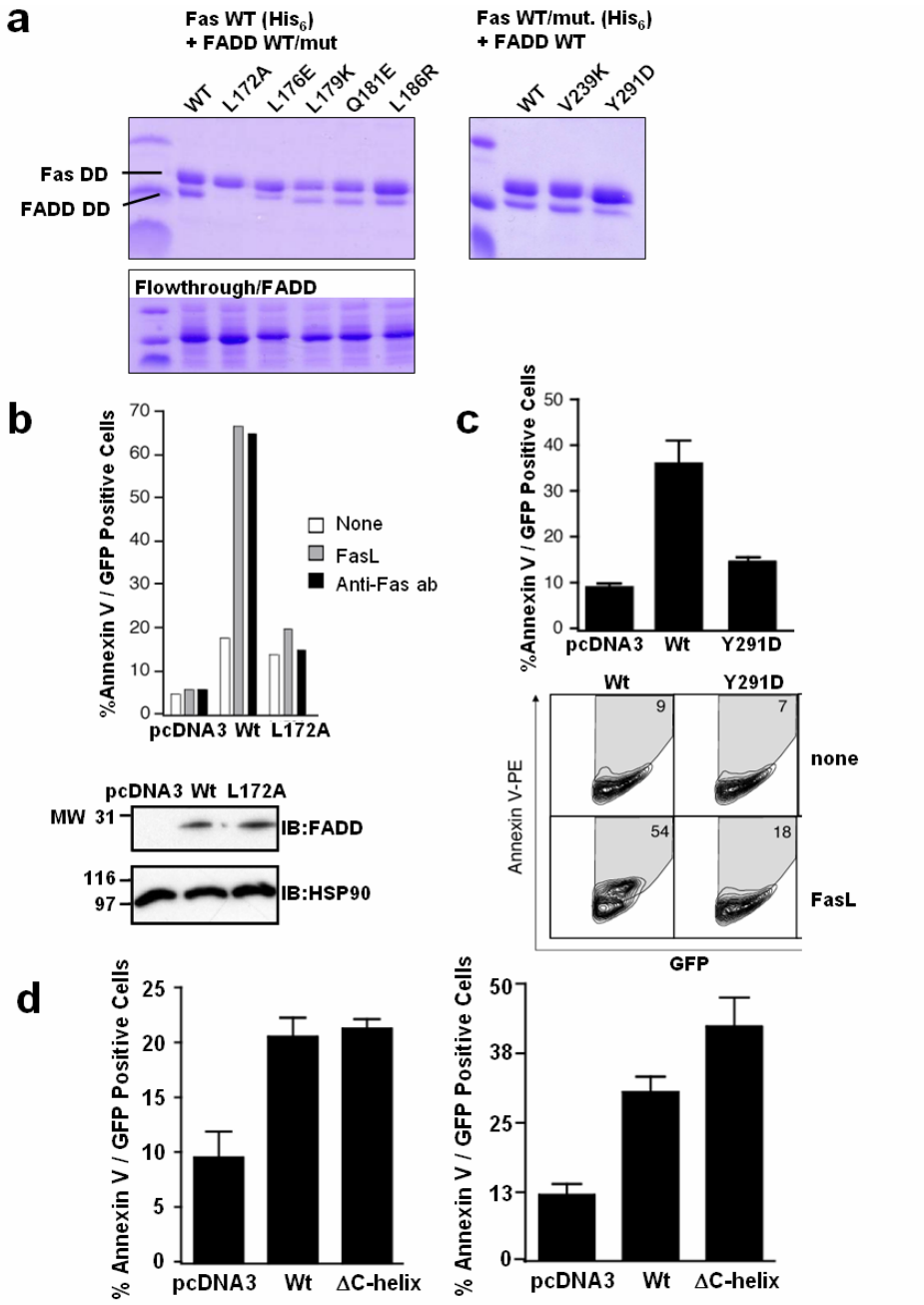

Supplementary Figure 3 | Mutational studies on the primary Fas/FADD interface. a, Complex Formation Assay. Fas/FADD interface mutants show only mild effects. Results from the complex formation assay of FADD and Fas mutants using His_6–Fas DD constructs and untagged FADD DD protein. To bypass the difficult nature of the Fas/FADD complex, binding was tested by complex formation in bacterial lysates of mutant and wild type (WT) proteins of Fas DD and FADD DD, followed by Ni-affinity chromatography. Ni-NTA beads were then analyzed by SDS-PAGE to assess complex formation (Coomassie staining). Various FADD interface mutants were tested, while mutational analysis of Fas residues in the interface was limited by their essential role in formation of the hydrophobic core of the death domain in the closed form. (left) Fas WT and

FADD WT/mutant proteins. Shown is retainment of FADD on the Ni-NTA beads due to successful binding of Fas. (the N-terminal His_6-tag on Fas DD gives a greater apparent MW than FADD DD). Interface mutant L172A exhibits a total loss of binding, L176E shows reduced binding, and the remaining mutants show no significant difference in the Fas to FADD ratio. (right) Fas-WT/mutants and FADD WT protein. The Y291D mutant of Fas shows reduced binding to FADD, while the V239K shows no difference in FADD binding compared to WT Fas. **b,** *In vivo* testing of FADD mutants**.** (top) Only interface mutant L172A results in a significant decrease in the induction of apoptosis relative to wild type. FADD deficient Jurkat cells (I2.1) were transfected with GFP and FADD mutants, treated with 100 ng/mL anti-Fas antibody or 100 ng/mL FasL for 3 hours and stained with Annexin V-PE. (bottom) Similar levels of protein expression compared to wild type were verified in a separate experiment. GFP positive cells were purified by FACSort, lysed in mRIPA, normalized for protein concentration, resolved by SDS-PAGE and immunoblotted with the indicated antibodies. Additional mutants tested were L176E, L179K, Q181E, L186R but these showed little or no significant reduction in apoptosis (data not shown). **c,** *In vivo* testing of Fas-mutants. Y291D reduces apoptosis. (top, standard deviations,n=3) Huh7 cells were transfected with GFP and Fas mutants and treated with 100 ng/mL anti-Fas antibody for 24 hours. (bottom) Huh7 cells were transfected with GFP and Fas mutants and treated with 100 ng/mL FasL for 3 hours. Grey box and number represent %GFP positive cells staining positive with Annexin V-PE. Additionally, the mutation of V239K had no significant effect on Fas killing (data not shown).

Both mutation of L172 in FADD and Y291 in Fas have been described previously[32, 33] and may additionally participate in globular interactions of the proteins (see Supplementary Figure 5b), since they reside in the periphery of the primary interface. Y291 was also implicated in endocytosis of Fas, but also shows reduced binding in our *in vitro* assay. **d.** The C-terminal helix of Fas shows neutral/adverse effects. Huh7 cells were transfected with GFP and wild type or truncated Fas (1-323) and treated with10 ng/mL FasL for 3 hours (left) or 100 ng/mL anti-Fas antibody for 24 hours (right) (standard deviations,n=3). FasL shows similar activity for both Fas proteins, while anti-Fas antibody treatment results in increased apoptosis of the truncated form. This effect was observed earlier in similar truncations and can be explained by the clash observed in the structural overlay.

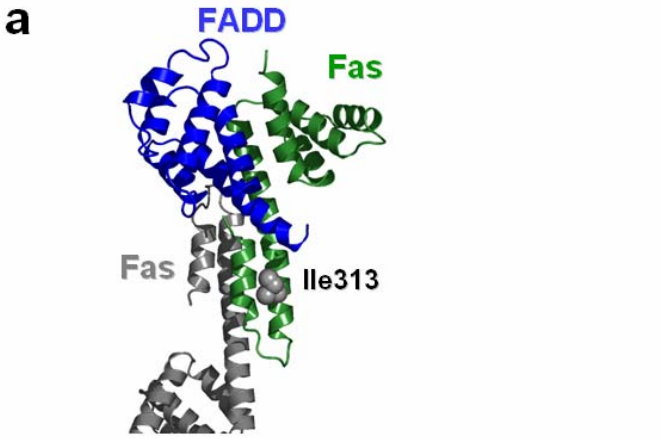

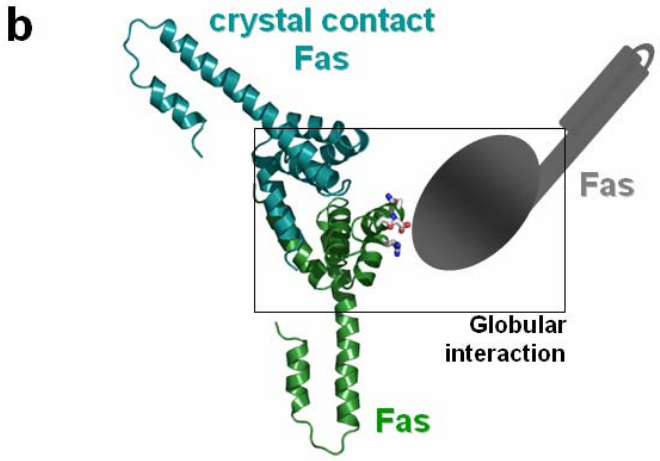

c

```
  fas    NLSDVD--L SKYITTIAGV MTLSQVKGFV RKNGVNEAKI DEIKNDNVQD TAEQKVQLLR
  dr4    NGADPTETL MLFFDKFANI VPFDSWDQLM RQLDLTKNEI DVVRAGTA-G PGDALYAMLM
  dr5    NEGDPTETL RQCFDDFADL VPFDSWEPLM RKLGLMDNEI KVAKAEAA-G HRDTLYTMLI
tnfR1    KPQSLDTDD PATLYAVVEN VPPLRWKEFV RRLGLSDHEI DRLELQNGRC LREAQYSMLA
```

stem helix

```
  fas    NWHQLHGK-K EAYDTLIKDL KKANLCTLAE KIQTIILKDI TSDSENSNFR NEIQSLV
  dr4    KWVNKTGR-N ASIHTLLDAL ERMEERHAKE KIQDLLVDSG KFIYLEDGTG SAVSLE
  dr5    KWVNKTGR-D ASVHTLLDAL ETLGERLAKQ KIEDHLLSSG KFMYLEGNAD SAMS
tnfR1    TWRRRTPRRE ATLELLGRVL RDMDLLGCLE DIEEALCGPA ALPPAPSLL
```

Supplementary Figure 4 | Opening of Fas: Ile313 - globular contacts – primary interface in other death receptors. a, Position of Ile313 in the Fas/FADD DD structure. Ile313 does not directly participate in the Fas/FADD (green/blue) interaction or the observed Fas/Fas dimer (green/grey) in the complex structure. The residue resides at the periphery of a hydrophobic patch formed by the stem helix and the C-helix, where it is located at the surface so that mutation to Asp should have marginal or no effect on this interaction. **b,** Globular interaction unit. Globular units of Fas interact utilizing surfaces described by mutations in earlier studies (Supplementary Table 2; reviewed in [5, 14]). Only one putative globular Fas/Fas unit contact is seen as a Fas/Fas crystal

contact in the structure, since these contacts were necessarily suppressed by utilizing acidic conditions to prevent clustering and allow for crystal formation (at identical pH used in the previously reported solution structure of the Fas DD[20]). The Fas molecules participating in this interaction are displayed in cyan and green. Additionally displayed are residues R250, N255, A257, D260, N264 of Fas, which are implicated in various diseases (see Supplementary Table 2). An additional Fas molecule is shown in cartoon representation (grey) illustrating a potential interaction site of the globular region of open Fas with the surface in which the disease mutants are located, schematically resulting in a Fas trimer. **c,** Primary complex interface of Fas: Conservation of hydrophobic residues on the DD of Fas, other FADD dependent death receptors and TNF-R1. Aligned are regions homologous to Fas residues 223-end. Hydrophobic residues providing the core of the primary interface for the complex on Fas and their homologous residues are visualized by red squares. The alignment shows that the hydrophobic character of all residues is fully maintained in DR4 and DR5, yet to a lesser degree in TNF-R1, which utilizes TRADD as primary binding partner. (Alignment was produced using Multalign [40].)

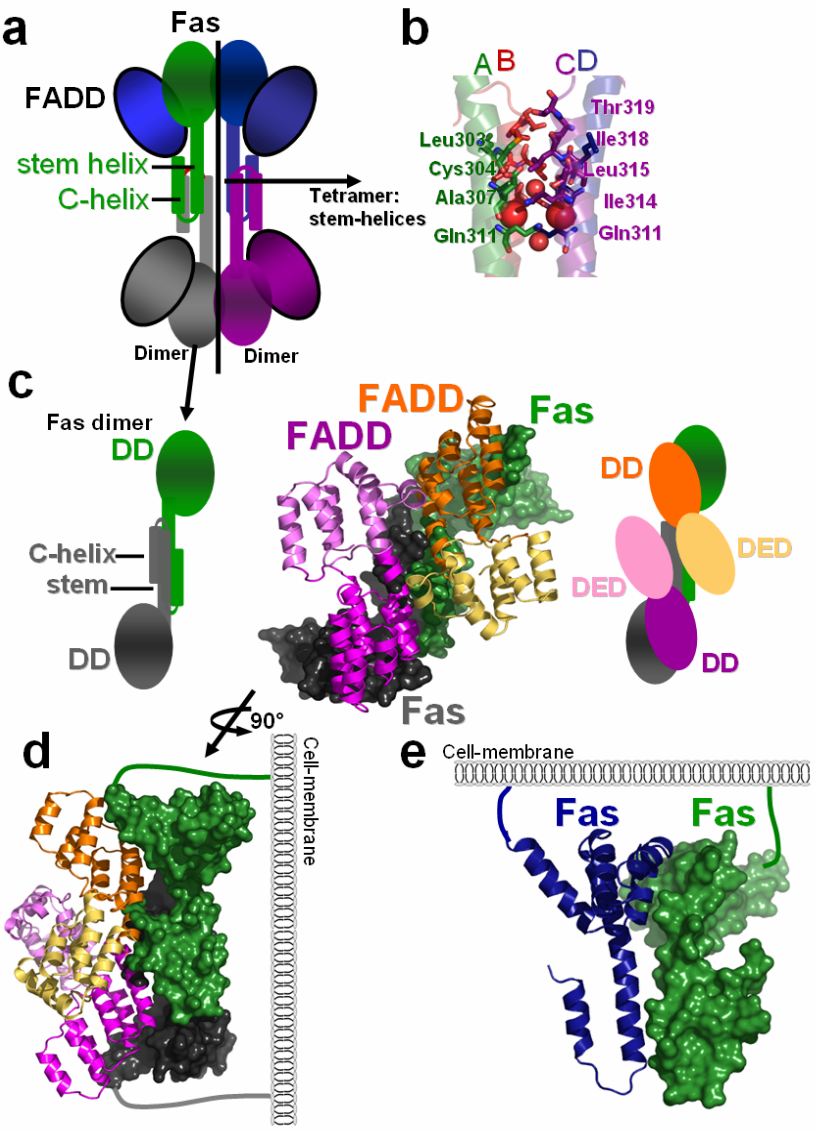

Supplementary Figure 5 | The Fas/Fas, Fas/FADD bridge in the DISC. a, Schematic of the isolated Fas/FADD DD complex in solution as observed in the crystal structure. **b,** The tetrameric interaction surface is built by a loose interaction of the four Fas stem helices which is interrupted by solvent molecules (here interpreted as sodium/water molecules (red)). **c,** Schematic of the observed Fas dimer (left) and the Fas dimer with two full length FADD* molecules (right). Full length molecules were overlayed (analogous to Fig. 3a) on the Fas dimer (middle). In addition to the primary interaction of the DD of FADD with Fas, further interactions of the DED of FADD with Fas and interactions of two Fas molecules are possible in this orientation. **d,** The observed dimeric unit is sterically more favorable than the tetramer in the context of a planar cell membrane. **e,** Other interactions of the open forms are possible in the formed DISC at the cell membrane. For example, illustrated here is the alternative stem

helix arrangement derived from the structure, that formed by the two Fas DDs which would represent a perpendicular orientation to the membrane.

SUPPLEMENTARY DISCUSSION

The Fas/FADD DD complex: The DISC at the membrane

The crystal structure of the Fas/FADD DD complex shows a tetrameric arrangement of four Fas/FADD DD complexes in which all contacts building the tetramer are provided by open Fas. Independent *in vitro* data confirms the existence of the tetramer in solution, strongly suggesting that the crystal structure of this complex, a key element of the DISC, reflects the shape of the Fas/FADD DD complex in solution. However, the actual DISC in the *in vivo* situation is a highly complex membrane dependent signaling platform, which is characterized by extensive clustering events and currently remains beyond detection on a molecular level. Yet the structure of the Fas/FADD DD complex as the key element of the DISC exposes the primary complex and gives rise to a mechanism of DISC formation as documented in the main body of this study. Does this primary complex also reveal structural details of the DISC as signaling clusters at the cell membrane and show, for example, how open Fas molecules interact within the DISC? In the *in vivo* situation and in the context of full length Fas, the DD is preceded by a transmembrane helix which (i) places steric limitation on the DD arrangements governed by the linker length and other factors such as Palmitoylation, and (ii) arranges the Fas DD into close proximity of the membrane. In the light of steric requirements on a planar membrane, a tetrameric unit appears unfavorable. The tetrameric arrangement of the Fas/FADD complex in solution may in fact resemble a result of the complex compensating for the lack of membrane interaction, thus binding to “itself”. Indeed, analysis of the structure points to a dimer of dimers, namely the association of two dimers formed by the stem-helices and C-helices of two Fas molecules, which in turn interact via their stem-helices in an anti-parallel manner to form the tetrameric arrangement (Supplementary Fig. 5 a-c).
Structurally, the dimer interface is preferred to the tetramer interface, which is loosely built by the four stem helices of Fas and is even interrupted by solvent molecules (Supplementary Fig. 5b), a feature that has been described to weaken helix interactions in the case of a yeast SNARE complex [41]. Thus the observed dimer more likely reflects the arrangement in the actual DISC. A consequential tandem arrangement of the two bound FADD molecules, illustrated in Supplementary Fig. 5c, furthermore would allow contacts of the DEDs of FADD to Fas as proposed in earlier studies, as well as additional FADD/FADD contacts. This arrangement (Supplementary Fig. 5c, d) would reflect an attractive connection between the presumed trimeric Fas modules (Supplementary Fig. 4b), although other arrangements are possible (Supplementary Fig. 5e). Complementary high end studies are required before conclusions on the structure of the membrane-bound DISC - beyond the primary Fas/FADD interaction and mechanism proposed in the main body of this work - can be drawn.

The Fas/FADD DD and other complexes of the death domain superfamily

The primary Fas/FADD death domain complex shows for the first time a unique element: an opening of the DD of Fas is directly used for the binding of the FADD DD. The implications of this feature, an interesting adaptation for a regulatory complex, are outlined and discussed in the main body of the study. But how does this observation relate to other complexes formed by members of the death domain superfamily? Historically, the first structural insight into a complex of this family was gained through the CARD/CARD complex of caspase-9 and Apaf-1. This complex shows a direct surface/surface interaction of both domains forming a constituent 1:1 complex [42]. Since death domains are regarded as adaptor domains and characteristic surface regions define individual types of death domains, such as CARD, DD, DED etc., this mode of binding was recognized as an attractive paradigm for other complexes of the death domain superfamily. Somewhat surprising in this context were the findings from the drosophila Pelle/Tube complex, where different surfaces were found to be involved in the DD interaction, and even more striking was the key role of residues adjacent to the actual DD [43]. The recent structure of the PIDD/RAIDD DD complex showed a surprising and unique 5:7 arrangement.[44] This complex also had to be generated by incubating the purified DD of PIDD and RAIDD at high concentrations at room temperature to reach this globular arrangement. Thus from a rigid defined constitutive 1:1 complex as seen in the Apaf-1/caspase-9 CARD/CARD interaction, the current views extend to plasticity and asymmetry of complexes in the death domain superfamily.[5]
Importantly, these differences may directly reflect the regulatory function of the parent complexes. The regulation of apoptosome signaling is mainly attributed to the nucleotide and cytochrome C dependent oligomerization of Apaf-1. The PIDDOSOME represents the middle ground where the LRR regions in coordination with the DDs participate in transmitting the oligomerization signal. The DISC however, as proximity induced conduit through the cell membrane is on the far end of the spectrum. Not only is this signaling platform peripheral to the cell membrane, but the signal on the cytosolic face of the membrane is solely mediated by DDs purely by proximity induced lateral clustering events. The solution to accommodate this complexity is a conformational change in Fas, which acts as the sensitive switch as shown by the crystal structure presented in this work.

Another line of thought concerning death domain superfamily complexes is the fact that while there are 86 human members of this superfamily, (32 of them DDs) [5] only these few complex structures are available, despite their crucial importance in key cellular processes such as apoptosis and inflammation.

This raises the question of whether other membrane dependent death receptors utilize a similar opening mechanism in their intracellular dearth domains as observed here for Fas/FADD. Naturally more detailed structural and mechanistic insights into complexes formed by these receptors are needed to answer this question. However, secondary structure predictions pointing to a long continuous helix in Fas and in the homologous regions of DR4 and DR5 suggest that these

regions also form long stem helices (data not shown). An additional interesting result is the conservation of hydrophobic residues, which build the interaction surface Fas utilizes to bind FADD, among Fas, DR4 and DR5 (Supplementary Fig. 4c). In comparison only a portion of these residues are of hydrophobic nature in the DD of TNF-R1, a receptor that utilizes TRADD and not FADD as primary adaptor. Thus it is feasible that DR4 and DR5 function by a similar mechanism as Fas, which remains to be seen in future structural and mechanistic studies.

Supplementary Table 1. Crystallographic Statistics

Data Set	**Native**	**Pt-SAD**
Source	NSLS-X29A	NSLS-X29A
Wavelength (Å)	1.100	1.100
Resolution range (Å)	30.00 – 2.73	30.00 – 3.00
Space group	P_{61}	P_{61}
Unit cell Native	a = b =126.22Å. c =299.27Å. α = β =90.00°. γ =120.00°	
Unit cell Pt-SAD	a = b =126.17Å. c =299.20Å. α = β =90.00°. γ =120.00°	
Reflections observed	662,154	474,139
Reflections unique	66,820	55,182
Completeness (%) (last shell)	98.7 (88.4)	93.8 (51.1)
I/σ (last shell)	9.3 (1.7)	6.6 (1.2)
R_{merge}[a] (%) (last shell)	7.6 (43.5)	9.0 (46.2)
Phasing		
Resolution range (Å)		30.0 – 4.2
Pt sites		11
FOM Solve		0.41
Refinement statistics		
Resolution range (Å)	30.00 – 2.73	
Reflections (total)	66,785	
R_{cryst}[b] / R_{free}[c] (%)	23.39 / 27.80	
Protein residues / atoms	1.964 / 13.785	
Sulfate and sodium ions	21	
Water molecules	231	
RMSD angles (°)	1.28	
RMSD bonds (Å)	0.016	
Average isotropic B-value	72.4 $Å^2$	

[a] $R_{merge} = \Sigma | I - < I > | / \Sigma I$, where I is the observed intensity and < I > is the average intensity from multiple observations of symmetry-related reflections, the value in parentheses correspond to the highest resolution shell. [b] $R_{cryst} = \Sigma | (Fobs)-(Fcalc) | / \Sigma (Fobs)$, [c] R_{free} = same as R_{cryst} but comprises a test set (5.1% of total Reflections), which was not used in model refinement.

Supplementary Table 2. Location of Fas DD Mutants Reportedly Affecting Complex Formation

Mutation[#]	Reported Effect*	Location in Complex Structure
Y232C	ALPS	helix1- primary Fas/FADD interaction site, possibly affecting fold of closed form
T241K	ALPS	linker-(helix1-2)- surface of Fas globular region
T241P	ALPS, loss of FADD binding[$,d]	linker-(helix1-2)- surface of Fas globular region
R250A	loss/reduced Fas self-association and FADD binding[c]	helix2- surface of Fas globular region
R250P	ALPS, loss of FADD binding[$,d,e]	helix2- surface of Fas globular region
R250Q	ALPS, loss of FADD binding[$,d]	helix2- surface of Fas globular region
V254N	leads to lpr in mice, affects Fas fold, loss/reduced Fas self-association and FADD binding[b,c,d]	linker-(helix2-3)- likely affecting core stability
N255D	squamous cell carcinoma, burn-scar related, somatic mutation	linker-(helix2-3)- surface of Fas globular region
E256A	loss/reduced Fas self-association and FADD binding[c]	linker-(helix2-3)- surface of Fas globular region
A257D	ALPS, loss of FADD binding[$,d]	linker-(helix2-3)- surface of Fas globular region
D260G	ALPS, loss of FADD binding[$,e]	helix3- surface of Fas globular region
D260V	ALPS, non-Hodgkin's lymphoma, somatic mutation, loss of FADD binding[$,d]	helix3- surface of Fas globular region
D260Y	ALPS, loss of FADD binding[$,d,e]	helix3- surface of Fas globular region
D260A	loss/reduced Fas self-association and FADD binding[c,f]	helix3- surface of Fas globular region
E261A	loss/reduced Fas self-association[c]	helix3- surface of Fas globular region(crystal contact)
K263A	loss/reduced Fas self- association[%,c,f]	helix3- surface of Fas globular region
N264K	non-Hodgkin's lymphoma, somatic mutation	helix3- surface of Fas globular region
T270I	ALPS[e]	helix4- surface of Fas globular region
E272G	ALPS	helix4- surface of Fas globular region(crystal contact)
E272K	non-Hodgkin's lymphoma, somatic mutation	helix4- surface of Fas globular region(crystal contact)
L278F	non-Hodgkin's lymphoma, somatic mutation	helix4- likely affecting core stability
D292A	no change to FADD interaction[c]	stem-helix- no interactions in complex
I310S	loss of FADD binding[$]	stem-helix- affects Fas-Fas dimer
K296A	reduced FADD binding[†]	stem-helix- adjacent to Fas tetramer interaction
K299N	non-Hodgkin's lymphoma, somatic mutation	stem-helix- localized in Fas dimer interaction
L315A	no change to FADD interaction[c]	stem-helix- localized in Fas tetramer interaction
truncated at: 225,230,246,250	loss of FADD binding[$,e]	eliminates all or a portion of helix2 of DD
truncated at: 273,276	loss of FADD binding[$,d]	eliminates a portion of helix4, stem-helix and C-helix
truncated at 294	loss of FADD binding[$,d]	eliminates a portion of stem-helix and C-helix
truncated at 312	loss of FADD binding[$,b]	eliminates a portion of stem-helix and C-helix
truncated at 320	enhanced FADD binding[a,b]	eliminates C-helix

[#]residue numbering and disease mutations according to swiss-prot entry: P25445
*described in terms of disease mutations and/or key-worded effect in published studies, for detailed information please see references cited below
[$] report does not probe Fas self-association, [%]also reported as having no effect on FADD interaction

a. Itoh, N., and Nagata, S. A novel protein domain required for apoptosis. *J Biol Chem* **268**, 10932-10937 (1993).
b. Chinnaiyan, A.M., O'Rourke, K., Tewari, M., and Dixit, V.M. FADD, a novel death domain-containing protein, interacts with the death domain of Fas and initiates apoptosis. *Cell* **81**, 505-512 (1995).
c. Huang, B., Eberstat, M., Olejniczak E.T., Meadows R.P., Fesik S.W. NMR structure and mutagenesis of the Fas (APO-1/CD95) death domain. *Nature* **384**, 638-641 (1996).

d. Martin, D.A., Zheng, L., Siegel, R.M., Huang, B., Fisher, G.H., Wang, J., Jackson, C.E., Puck, J.M., Dale, J., Straus, S.E., Peter, M.E., Krammer, P.H., Fesik, S., and Lenardo, M.J. Defective CD95/APO-1/Fas signal complex formation in the human autoimmune lymphoproliferative syndrome, type Ia. *Proc Natl Acad Sci USA* **96**, 4552-4557 (1999).
e. Vaishnaw, A.K., Orlinick, J.R., Chu, J., Krammer, P.H., Chao, M.V., and Elkon, K.B. The molecular basis for apoptotic defects in patients with CD95 (Fas/Apo-1) mutations. *J. Clin. Invest.* **103**, 355-363 (1999).
f. Ferguson, B.J., Esposito, D., Jovanovic, J., Sankar, A., Driscoll, P.C., and Mehmet, H. Biophysical and cell-based evidence for differential interactions between the death domains of CD95/Fas and FADD. *Cell Death Differ* **14***,* 1717-1719 (2007).

SUPPLEMENTARY METHODS

Protein Expression, Co-purification, and *in vitro* Complex Formation Assays.

For crystallization and analysis of the complex, Fas DD (residues 223–335; EMBL: M67454) and FADD DD (residues 93–208; EMBL: U24231) were cloned into bacterial expression vectors (pet-29, EMD) using standard PCR methods. The resulting Fas DD construct was untagged and contained the additional amino-acids Leu-Glu at the C-terminus, and the FADD DD construct contained a C-terminal His_6-tag. After expression of the individual proteins in *E. coli*, the cell lysates (in 50 mM Tris pH 8.0, 100 mM NaCl, 10% glycerol) were combined to form the Fas/FADD DD complex, which was then purified using Ni-NTA affinity resin (Qiagen). The complex was further purified and separated from excess un-complexed FADD DD by ion-exchange chromatography (SourceQ 10/10 column, GE Healthcare). Isolated complex was typically obtained at concentrations in the range of 10 mg/mL. Furthermore, complex formation was also performed by co-expression of identical constructs in pet29 and pACYC duet (EMD) derivatives, which yielded identical Fas/FADD DD complexes as judged by ion-exchange and gel filtration (data not shown).

For complex formation assays of Fas/FADD by co-purification, Fas (223-335) constructs were generated resulting in a DD with an N-terminal His_6-tag (pet-28, EMD) and an untagged FADD DD (pet-29, EMD). Binding of full length FADD to Fas was investigated using C-terminal His_6-tagged FADD (F25Y)* [18, 34] and untagged Fas DD. Expression and co-purification was performed analogous to the procedure described above, with binding assessed by SDS-PAGE analysis of bound protein on the Ni-NTA beads.

*F25Y is a well documented solubility mutant, which was used for FADD full length data and is generally utilized for *in vitro* studies involving the DED of FADD[18,34].

Crystallization of the Fas/FADD DD Complex.
Isolated complex (~10 mg/mL) in 10 mM Hepes, ~300 mM NaCl, 2 mM DTT, pH 7.8 post ion-exchange purification was used directly for crystallization. In the successful condition, 2.2 µL of protein solution was mixed with 2 µL of reservoir solution 0.95 M citric acid, 1.9 M ammonium sulfate resulting in a final pH of 4. Initial crystals appeared after 8 to 15 days at 4 °C and were further improved using micro and macro-seeding techniques combined with a 3 week aging step, resulting in diffracting crystals with dimensions up to 0.2 x 0.2 x 0.2 mm^3. Derivative crystals for phasing were obtained by soaking crystals for 3 hours in 3 mM $K_2Pt(CN)_4$. Prior to measurement crystals were flash frozen with 18% glycerol as cryo-protectant.

Structure Determination and Analysis.
Anomalous and native diffraction data were collected at the National Synchrotron Light Source on beamline X29 at wavelengths corresponding to the peak of a Pt-SAD experiment. The data sets were collected at 100 K using ADSC Quantum 315 CCD detector. Data were integrated, reduced and scaled with HKL2000[35]. The initial structure was determined from the 4.5 Å Pt-SAD data using SOLVE/RESOLVE[36]. Model building and TLS-refinement were performed with the 2.73 Å native dataset using O[37] and REFMAC5[38]. Tight and medium NCS restraints were imposed for main- and side-chain atoms, respectively. Data collection and refinement statistics are summarized in Supplementary Table 1 (above).
The final model includes two sets of tetrameric (four) Fas/FADD complexes, 13 sulfate and 8 sodium ions, as well as 231 water molecules in the asymmetric unit. For all Fas chains the model includes residues 223-335 of Fas and the additional Leu-Glu sequence. The model for all FADD chains includes residues 93-191 of the protein. Weak electron density was observed for FADD residues 107-149 in all FADD chains. The model exhibits excellent stereochemical quality as validated by the AutoDepInputTool (http://deposit.pdb.org/adit/). Figures were prepared with PYMOL (DeLano Scientific).

Analysis of the Fas/FADD Death Domain Complex.
For gel filtration analysis the isolated Fas/FADD DD complex (200 µL) post ion-exchange chromatography was applied to a Superdex S75 column with 20 mM Hepes, 100 mM NaCl, 2 mM DTT as running buffer followed by analysis of the fractions using standard SDS-PAGE. For analysis of the isolated complex by size limiting pore gel electrophoresis, native gels with a gradient from 6-32% poly acrylamide were run for 16 hours at RT to allow all protein/complex species to migrate to their size limit. The proteins CrmA, BSA and Transferrin were used for size reference.
To evaluate the stability of the complex, isolated Fas/FADD DD complex (with only FADD DD containing a His_6-tag) was purified by ion-exchange chromatography (as described above but in the absence of DTT) and protein concentration of the complex fraction was determined using absorption at 280 nm. The complex was then diluted to different final concentrations at a final

volume of 40 µL then mixed with 40 µL of Ni-NTA resin and eluted with imidazole after a rapid wash step. Protein was visualized on an SDS-PAGE and the Fas to FADD ratio concluded by analysis of background corrected band intensity on a CCD-based System Alpha Imager 2200 (Alpha Innotech) using the AlphaEase software.

For analysis of the Fas/FADD DD complex by analytical ultracentrifugation, sedimentation equilibrium experiments were performed in a ProteomeLab XL-I (BeckmanCoulter) analytical ultracentrifuge. Complex samples after Ion-exchange were diluted in buffer (10 mM Hepes, ~300 mM NaCl, 2 mM DTT, pH 7.8) to final concentrations of 370, 125, 13, 4.5 and 1.5 µM, loaded in 6-channel equilibrium cells and spun in an An-50 Ti 8-place rotor at 12,000 rpm, 20 ^{o}C for 24 hours. Since some of the concentrations used were out of range for detection using an absorption system, a Rayleigh interference system was used for detection. Data were analyzed using HeteroAnalysis software (by J.L. Cole and J.W. Lary, University of Connecticut).

In vivo Analysis of Fas/FADD Wild type and Mutants

Plasmids, Cell Culture, Transfections and Apoptosis Assays.

Full length Fas in pcDNA3 was a kind gift from Dr John Reed (Burnham Institute for Medical Research, La Jolla, California). Full length FADD was subcloned into pcDNA3.1/Hygro (Invitrogen) using standard techniques. pEGFP was from Clontech. All mutants were created using Quickchange (Stratagene) and confirmed by sequencing across both strands.

Huh7 cells were cultured in DMEM with 10% FBS, 2 mM glutamine, penicillin/streptomycin, 10 mM Hepes and non-essential amino acids. Jurkat FADD negative (I2.1) cells (ATCC) were cultured in RPMI with 10% FBS, 2 mM glutamine, penicillin/streptomycin, 10 mM Hepes, 1 mM Na-Pyruvate, 4.5 g/L glucose and 1.5 g/L Na-bicarbonate. All cells were transfected with GeneJuice (Novagen) according to manufacturers instructions.

For apoptosis assays, Huh7 cells were transfected with 25 ng GFP, 250 ng Fas mutant and 750 ng pcDNA3. Jurkat I2.1 cells were transfected with 250 ng GFP, 1 µg FADD mutant and 3.75 µg pcDNA3. 24 hours post transfection, cells were treated with anti-Fas (clone CH11) antibody (Upstate) or FasL with Enhancer (5x the FasL concentration; Alexis Biochemicals). Cells were stained with Annexin V-PE (Caltag) and analyzed by flow cytometry. Apoptotic cells were expressed as the percentage of GFP positive cells showing Annexin V-PE staining.

For detection of FADD expression in transfected Jurkat deficient (I2.1) cells, 4 x 10^6 cells were transfected with 1 µg FADD variant, 0.25 µg GFP and 3.75 µg pcDNA3, and purified by FACSsort using a FACSDiVa (Becton Dickinson) for GFP positive cells (approximately 2% total cell population).

To evaluate cell surface Fas expression, Huh7 cells were transfected with 1 µg Fas variants for 24 hours. Cells were detached with 5 mM EDTA, 1% (w/v) BSA in PBS. Cells were washed twice in wash buffer (0.5% (w/v) BSA in PBS) and fixed with 3.8% (v/v) formaldehyde for 10 min at room temperature. Cells were chilled on ice, washed twice with wash buffer, stained with 1 µg/mL mouse anti-

Fas antibody (clone 2R2; Biosource) for 1 hour at RT, FITC-conjugated anti-mouse IgG (Molecular Probes) for 30 min at room temperature, washing three times with wash buffer between each incubation. Cells were analyzed by flow cytometry for FL1 fluorescence.

Electrophoresis and Immunoblotting.
Samples were lysed in ice cold mRIPA buffer containing protease inhibitors, analyzed by 8-18% linear gradient acrylamide SDS-PAGE under reducing conditions and immunoblotting was as described (Denault and Salvesen, 2003). Antibodies were mouse anti-Fas antibody (clone 3D5; Alexis Biochemicals), mouse anti-HSP90 (BD Transduction Laboratories), mouse anti-FADD (A66-2; BD Pharmingen), and HRP-conjugated donkey anti-mouse IgG (Amersham Biosciences).

Electron Microscopy.
Negative staining of protein; 5 µL of the Fas/FADD protein (~5 ug/mL) in 20 mM Tris pH 8.0, 100 mM Nacl was placed on the surface of carbon coated grids (EMS, Hatfield, PA), sedimented for 1 minute, and the extra solution was blotted off. 5 µL of 2.0% uranyl-acetate in ddH_2O was added over absorbed particles and incubated for 30 seconds. Extra staining solution was then blotted off. Air dried samples were observed in the transmission electron microscope Hitachi H-600A, at 75 kV and X100,000 instrumental magnification. Images were acquired with the 11.2 megapixel digital cooled CCD camera SIA-L9C (Atlanta, GA) controlled by Maxim DL, v.4.56 imaging software (Cyanogen Imaging Products, Ottawa, Ontario, Canada).

SUPPLEMENTARY REFERENCES

31. Fawcett, J. S., Sullivan, J. V. & Chrambach, A. Toward a steady-state pore limit electrophoresis dimension for native proteins in two-dimensional poly acrylamide gel electrophoresis. *Electrophoresis* **10**, 182-5 (1989).

32. Hill, J. M. et al. Identification of an expanded binding surface on the FADD death domain responsible for interaction with CD95/Fas. *J Biol Chem* **279**, 1474-81 (2004).

33. Lee, K. H. et al. The role of receptor internalization in CD95 signaling. *Embo J* **25**, 1009-23 (2006).

34. Eberstadt, M. et al. NMR structure and mutagenesis of the FADD (Mort1) death-effector domain. *Nature* **392**, 941-5 (1998).

35. Otwinowski, Z. & Minor, W. [20] Processing of X-ray diffraction data collected in oscillation mode. *Methods in Enzymology* **276**, 307-326 (1997).

36. Terwilliger, T. C. & Berendzen, J. Automated MAD and MIR structure solution. *Acta Crystallogr D Biol Crystallogr* **55**, 849-61 (1999).

37. Jones, T. A., Zou, J. Y., Cowan, S. W. & Kjeldgaard, M. Improved methods for building protein models in electron density maps and the location of errors in these models. *Acta Crystallogr A* **47** (Pt 2), 110-9 (1991).

38. Murshudov, G. N., Vagin, A. A. & Dodson, E. J. Refinement of macromolecular structures by the maximum-likelihood method. *Acta Crystallogr D Biol Crystallogr* **53**, 240-55 (1997).

39. Tobi, D. & Bahar, I. Structural changes involved in protein binding correlate with intrinsic motions of proteins in the unbound state. *Proc Natl Acad Sci U S A* **102**, 18908-13 (2005).

40. CORPET, F. Multiple sequence alignment with hierarchical clustering. *Nucl. Acids Res.* **16** (22), 10881-10890 (1988)

41. Strop, P., Kaiser, S. E., Vrljic, M. & Brunger, A. T. The structure of the yeast plasma membrane SNARE complex reveals destabilizing water-filled cavities. *J Biol Chem* **283**, 1113-9 (2008).

42. Qin, H. et al. Structural basis of procaspase-9 recruitment by the apoptotic protease-activating factor 1. Nature 399, 549-57 (1999).

43. Xiao, T., Towb, P., Wasserman, S. A. & Sprang, S. R. Three-dimensional structure of a complex between the death domains of Pelle and Tube. *Cell* **99**, 545-55 (1999).

44. Park, H. H. et al. Death domain assembly mechanism revealed by crystal structure of the oligomeric PIDDosome core complex. *Cell* **128**, 533-46 (2007).